Pergamon

Int. J. Solids Structures Vol. 35, Nos 28–29, pp. 3655–3674, 1998

0020–7683/98 $19.00 + .00

PII: S0020–7683(97)00215–1

DIFFERENTIAL CUBATURE METHOD FOR STATIC SOLUTIONS OF ARBITRARILY SHAPED THICK PLATES

F.-L. LIU and K. M. LIEW

Division of Engineering Mechanics, School of Mechanical and Production Engineering, Nanyang Technological University, Nanyang Avenue, Singapore 639798

(*Received* 20 *October* 1996; *in revised form* 21 *July* 1997)

Abstract—This paper presents the first endeavor to exploit the differential cubature method as an accurate and efficient global technique for fundamental solutions of arbitrarily shaped thick plates. The method is examined here for its suitability for solving the boundary-value problem of thick plates governing by the first-order shear deformation theory. Using the method, the governing differential equations and boundary conditions are transformed into sets of linear algebraic equations. Boundary conditions are implemented through discrete grid points by constraining displacements, bending moments and rotations. Detailed discussion on the formulation and implementation of the method are presented. The applicability, efficiency and simplicity of the method are demonstrated through solving example plate problems of different shapes. The accuracy of the method is verified by direct comparison with the known values. © 1998 Elsevier Science Ltd. All rights reserved.

1. INTRODUCTION

Thick plates are important structural elements which are used in a wide range of applications, including ship hulls, covers for cylinders, water tanks, doors of bunkers and hangars and armor plates for military vehicles and tanks. For some simple plate shapes and boundary conditions, exact or analytical solutions to these problems are possible. Apart from these, approximate methods are usually employed for the solutions of plates of arbitrary shape and with complicated boundary conditions.

With the modern computer technology, various numerical methods were well developed and widely used to solve various kinds of engineering problems which are described by the partial differential equations. Among them, the finite element method (FEM), the finite differential method (FDM) and the boundary element method (BEM) are the most powerful numerical tools and well established. These numerical methods are able to provide accurate results if the distribution of meshes is properly selected and a large number of grid points are used. However, in most practical circumstances, the moderately accurate solutions are desired at only a few specific points of the physical domain for rapid evaluation. In order to achieve the solutions even at or around a point of interest with moderate accuracy, the classical numerical methods such as FEM and FDM are still requiring a large number of grid points. As a result, the computational efforts and costs in mesh refining are usually unnecessarily large in such cases.

To cut down the computational cost for global problems, the differential quadrature (DQ) method was introduced (Bellman and Casti, 1971, 1972) and is now being actively researched in its development and application to the structural mechanics analysis (Bert *et al.*, 1988, 1989; Pandya and Sherbourne, 1991; Striz *et al.*, 1994; Liew *et al.*, 1996). However, the applications of DQ method as mentioned above were restricted to problems in rectangular variable domain. In order to extend the DQ method for solution of problems to non-rectangular domain, Shu and Chew (1994) adopted the curvilinear coordinates and combined with the DQ method to solve the in-compressible Navier–Stokes equations. The DQ method was further developed for bending analysis of Reissner/Mindlin plates with arbitrary quadrilateral geometry (Liew and Han, 1997) and straight or curvilinear boundaries (Han and Liew, 1997) by using the geometric coordinate mapping technique. Either

of them needs to make coordinate transformations. If the orders of the differential equations are higher than three, the transformations become complicated and cumbersome.

To overcome the above difficulty, Civan (1994) introduced a novel numerical technique, the differential cubature (DC) method as an accurate alternative to the differential quadrature method when dealing with multi-dimensional differential equations. The DC method is a direct discretization method which approximates the partial derivatives of a function by means of polynomials which expressed as a weighted linear sum of the function values at the grid points in the domain. The practical importance of the DC method is that it needs to use only a few grid points which is able to obtain an acceptable accuracy in an arbitrary domain. Besides, the DC method is much simpler than the DQ method when treating the multidimensional problems. Although the DQ method is also applicable to multivariate problems as shown by Civan and Sliepcevich (1984), it is most suitable for one variable problem, since it is based on a weighted linear sum of discrete function values in a single variable. The DC method includes the effect of various variables in numerical approximation. Civan (1994), in his publication, has shown that the DC method is exceptionally efficient in solving the mathematical models of Buckley-leverett problem for water flooding of naturally fractured oil bearing reservoirs and that the DC method is particularly advantageous over the DQ method when dealing with mixed operations, such as $\partial^2/\partial x\partial y$ and $(\partial/\partial x)\int\partial y$. Therefore it has been claimed to be a superior numerical method for solving the multi-dimensional problems. However, till now, the potential of this method for solution of a varied class of problems has not been explored and no other work on the application of the DC method to the structural mechanics field has been reported except for the authors recently made the first endeavor in using the DC method to solve partial differential equations in Kirchhoff plate bending problem (Liew and Liu, 1997). The numerical results (Liew and Liu, 1997) showed that the DC method yields rapid and converged numerical solutions and the results were in excellent agreement with the exact analytical solutions. With the encouragement of the previous studies (Civan, 1994; Liew and Liu, 1997), the authors are now further exploiting the potential applications of the DC method for modeling a thick plate bending problem in a systematic way.

This paper is organized into several sections. In Section 2, we provide the details of the DC method. In Section 3, we introduce the concept of DC procedures for bending analysis of thick plates using the first-order shear deformation theory (Reissner, 1945; Mindlin, 1951). In Section 4, the ease of use, and the convergence properties and accuracy of the DC method are demonstrated through the solving of numerical test examples for which the exact analytical solutions are available for comparison. Finally the conclusions from this study are drawn in Section 5.

2. DIFFERENTIAL CUBATURE METHOD

Basically the differential cubature method is a numerical procedure expressing a linear operation such as a continuous function or any orders of partial derivatives of multivariable function as a weighted linear sum of discrete function values chosen within the overall domain of interest of a problem (Civan, 1994). For a two-dimensional problem, the cubature approximation at the ith discrete point is given by

$$\mathscr{R}\{f(x,y)\}_i \cong \sum_{j=1}^{n} c_{ij} f(x_j,y_j) \tag{1}$$

where $\mathscr{R}$ denotes a linear differential operator which can be any orders of partial derivatives or the combinations of these partial derivatives, i is the one dimensional index of arbitrarily sequenced grid points for the two-dimensional solution domain shown in Figs 1–5, n is the total number of discrete points considered, and c_{ij} is the cubature weighting coefficients determined by the following expression

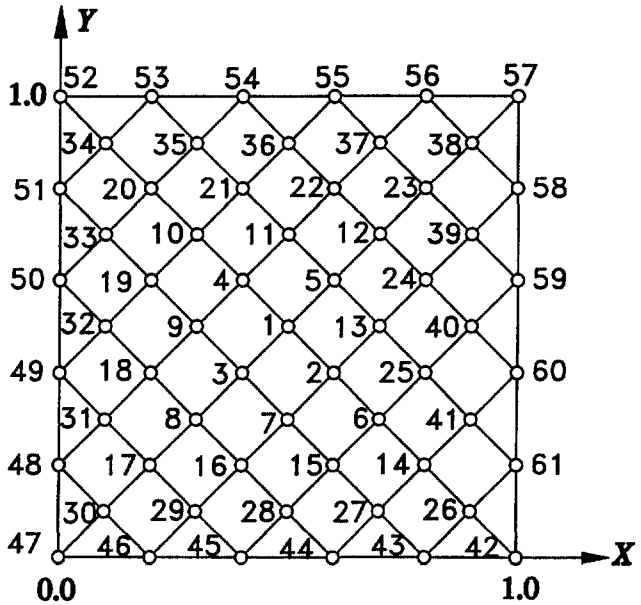

Fig. 1. The grid point pattern for rectangular plate problem.

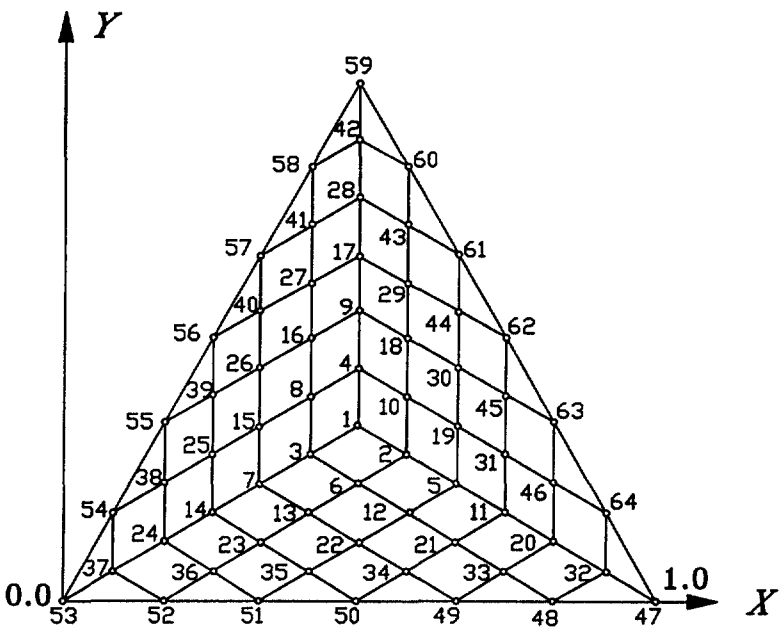

Fig. 2. The grid point pattern for triangular plate problem.

$$\mathscr{R}\{x^{\nu-\mu}y^{\mu}\}_i = \sum_{j=1}^{n} c_{ij}(x_j^{\nu-\mu}, y_j^{\mu}); \quad \mu = 0,1,2,\ldots,\nu; \quad \nu = 0,1,2,\ldots,k-1 \tag{2}$$

where $i = 1,2,3,\ldots,n$; or if written in a matrix form, eqn. (2) becomes

$$[x_j^{\nu-\mu}y_j^{\mu}] \begin{bmatrix} c_{i1} \\ c_{i2} \\ \vdots \\ c_{in} \end{bmatrix} = \mathscr{R}\{x^{\nu-\mu}y^{\mu}\}_i \tag{3}$$

in which $j = 1,2,3,\ldots,n$.

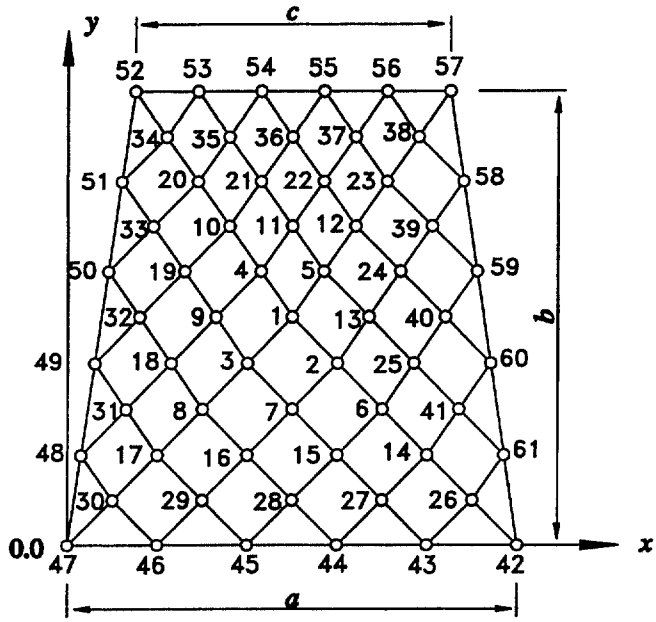

Fig. 3. The grid point pattern for trapezoidal plate problem.

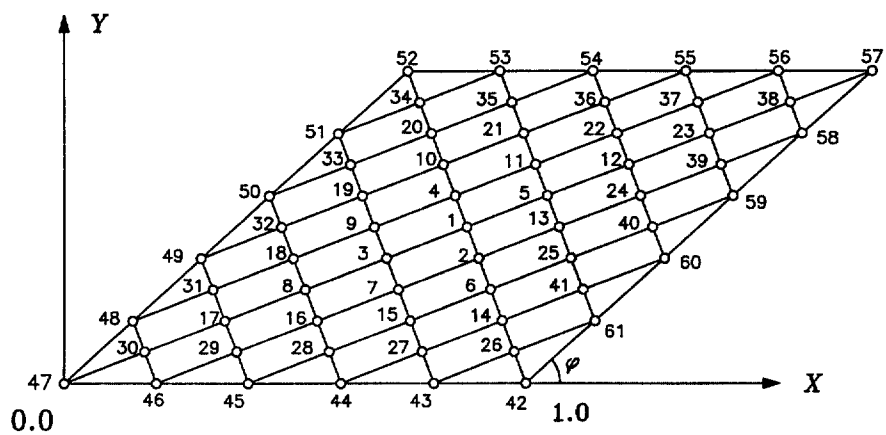

Fig. 4. The grid point pattern for skew plate problem.

The n-monomials, $x^{\nu-\mu}y^{\mu}$, are selected from a set of monomials which is used to obtain a unique solution of eqn (3). These monomials are given as follows:

$$
\begin{aligned}
&\nu = 0 && 1\\
&\nu = 1 && x \quad y\\
&\nu = 2 && x^2 \quad xy \quad y^2\\
&\nu = 3 && x^3 \quad x^2y \quad xy^2 \quad y^3\\
&\vdots && \cdots \quad \cdots \quad \cdots \quad \cdots \quad \cdots \quad \cdots \quad \cdots \quad \cdots\\
&\nu = k-1 && x^{k-1} \quad \cdots \quad \cdots \quad \cdots \quad x^{\nu-\mu}y^{\mu} \quad \cdots \quad \cdots \quad \cdots \quad y^{k-1}
\end{aligned}
\tag{4}
$$

Once the grid points (x_i, y_i) are given, the cubature weighting coefficients c_{ij} can be obtained by solving an $n \times n$ order linear algebraic equations.

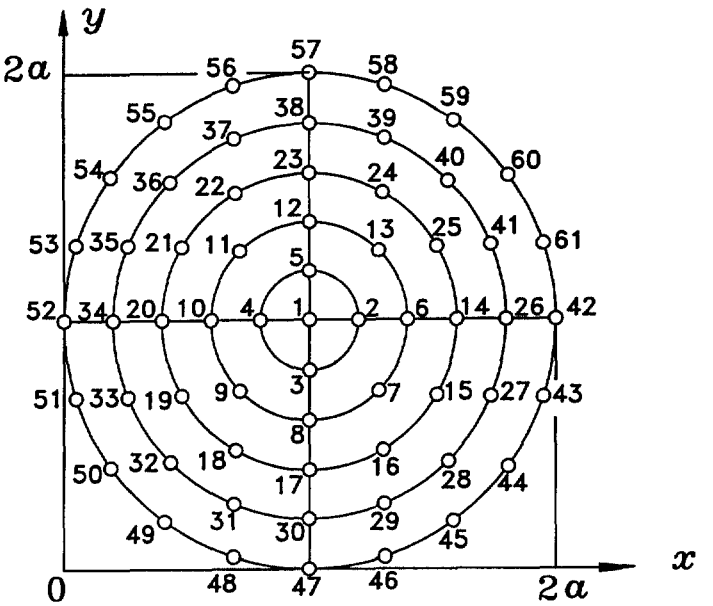

Fig. 5. The grid point pattern for circular plate problem.

3. MODELING OF THICK PLATES

3.1. *Basic governing equations*

Consider a thick, homogeneous and isotropic plate, the equilibrium governing equations are given in terms of the displacement components as follows (Kobayashi and Sonoda, 1989):

$$\frac{D}{2}\left[(1-\nu)\nabla^2\psi_x+(1+\nu)\frac{\partial\phi}{\partial x}\right]+\kappa Gh\left(\frac{\partial w}{\partial x}-\psi_x\right)=0 \tag{5a}$$

$$\frac{D}{2}\left[(1-\nu)\nabla^2\psi_y+(1+\nu)\frac{\partial\phi}{\partial y}\right]+\kappa Gh\left(\frac{\partial w}{\partial y}-\psi_y\right)=0 \tag{5b}$$

$$\kappa Gh(\nabla^2 w-\phi)+q=0 \tag{5c}$$

where

$$\phi=\frac{\partial\psi_x}{\partial x}+\frac{\partial\psi_y}{\partial y} \tag{6}$$

$$D=\frac{Eh^3}{12(1-\nu^2)} \tag{7}$$

and w is the transverse deflection; ψ_x and ψ_y are the rotations of the normal about the x-axis and y-axis respectively; D is the plate flexural rigidity; E is the Young's modulus; G is the shear modulus; ν is the Poisson's ratio; κ is the shear correction factor taken as 5/6; ∇^2 is Laplace's two-dimensional operator; and q is the upper surface load intensity.

The bending moments and twisting moments can be expressed as:

$$M_x=-D\left(\frac{\partial\psi_x}{\partial x}+\nu\frac{\partial\psi_y}{\partial y}\right) \tag{8}$$

$$M_y=-D\left(\nu\frac{\partial\psi_x}{\partial x}+\frac{\partial\psi_y}{\partial y}\right) \tag{9}$$

$$M_x = -\frac{1-\nu}{2}D\left(\frac{\partial \psi_x}{\partial y}+\frac{\partial \psi_y}{\partial x}\right) \tag{10}$$

The shear resultants can be expressed as:

$$Q_x = \kappa Gh\left(\frac{\partial w}{\partial x}-\psi_x\right) \tag{11}$$

$$Q_y = \kappa Gh\left(\frac{\partial w}{\partial y}-\psi_y\right) \tag{12}$$

To normalize the above equations, the following non-dimensional parameters are introduced:

$$X=\frac{x}{a};\quad Y=\frac{y}{b};\quad W=\frac{w}{h};\quad \Psi_X=\psi_x;\quad \Psi_Y=\psi_y \tag{13a–e}$$

$$\beta=\frac{a}{b};\quad \gamma=\frac{h}{b};\quad \delta=\frac{h}{a};\quad Q_d=\frac{q}{\kappa G\delta};\quad \xi=\frac{6\kappa(1-\nu)}{\delta^2}; \tag{13f–j}$$

where a and b are the length and width of the plate to be analysed along x-axis and y-axis, and Q_d is the normalized distributed load.

Substituting eqn (13) into eqn (5), normalizing and rearranging them, we obtain

$$\frac{\partial^2 \Psi_X}{\partial X^2}+\frac{(1-\nu)}{2}\beta^2\frac{\partial^2 \Psi_X}{\partial Y^2}-\xi\Psi_X+\frac{(1+\nu)}{2}\beta\frac{\partial^2 \Psi_Y}{\partial X\partial Y}+\xi\delta\frac{\partial W}{\partial X}=0 \tag{14a}$$

$$\frac{(1+\nu)}{2}\beta\frac{\partial^2 \Psi_X}{\partial X\partial Y}+\beta^2\frac{\partial^2 \Psi_Y}{\partial Y^2}+\frac{(1-\nu)}{2}\frac{\partial^2 \Psi_Y}{\partial X^2}-\xi\Psi_Y+\xi\gamma\frac{\partial W}{\partial Y}=0 \tag{14b}$$

$$\left(\delta\frac{\partial^2 W}{\partial X^2}+\gamma\beta\frac{\partial^2 W}{\partial Y^2}\right)-\left(\frac{\partial \Psi_X}{\partial X}+\beta\frac{\partial \Psi_Y}{\partial Y}\right)+Q_d=0 \tag{14c}$$

Substituting eqn (13) into eqns (8–10), the bending moments are normalized as follows:

$$\bar{M}_X = -\left(\frac{\partial \Psi_X}{\partial X}+\nu\beta\frac{\partial \Psi_Y}{\partial Y}\right) \tag{15a}$$

$$\bar{M}_Y = -\left(\nu\frac{\partial \Psi_X}{\partial X}+\beta\frac{\partial \Psi_Y}{\partial Y}\right) \tag{15b}$$

$$\bar{M}_{XY} = -\frac{1-\nu}{2}\left(\beta\frac{\partial \Psi_X}{\partial Y}+\frac{\partial \Psi_Y}{\partial X}\right) \tag{15c}$$

where, $\bar{M}_X = M_x/(D/a)$; $\bar{M}_Y = M_y/(D/a)$; $\bar{M}_{XY} = \mathrm{M}_{xy}/(D/a)$.

Similarly, substituting eqn (13) into eqns (11) and (12), the normalized shear resultants are given as:

$$\bar{Q}_X = \left(\delta\frac{\partial W}{\partial X} - \Psi_X\right) \tag{16a}$$

$$\bar{Q}_Y = \left(\gamma\frac{\partial W}{\partial Y} - \Psi_Y\right) \tag{16b}$$

where, $\bar{Q}_X = Q_X/(\kappa Gh)$, $\bar{Q}_Y = Q_Y/(\kappa Gh)$.

3.2. *Boundary conditions*

The boundary conditions for an arbitrary edge can be represented by the following equations:

• *Clamped edge* (C):

$$w = 0; \quad \psi_n = 0; \quad \psi_s = 0 \tag{17}$$

• *Simply supported edge* (S):

$$w = 0; \quad M_n = 0; \quad \psi_s = 0 \tag{18}$$

Representing the deformation variables and the force resultants in eqns (17–18) by their components along x-axis and y axis yields:

• *Clamped edge* (C):

$$w = 0 \tag{19a}$$

$$\psi_x\bar{n}_x + \psi_y\bar{n}_y = 0 \tag{19b}$$

$$-\psi_x\bar{n}_y + \psi_y\bar{n}_x = 0 \tag{19c}$$

• *Simply supported edge* (S):

$$w = 0 \tag{20a}$$

$$M_x\bar{n}_x^2 + M_y\bar{n}_y^2 + 2M_{xy}\bar{n}_x\bar{n}_y = 0 \tag{20b}$$

$$-\psi_x\bar{n}_y + \psi_y\bar{n}_x = 0 \tag{20c}$$

where in eqns (17–20), $\bar{n}$ denotes the normal direction of the edge; $\bar{n}_x$ and $\bar{n}_y$ represent the components of unit normal vector of the edge.

Substituting eqns (8–9) into eqns (19–20) and normalizing them using eqn (13) yields

• *Clamped edge* (C):

$$W = 0 \tag{21a}$$

$$\Psi_X\bar{n}_x + \Psi_Y\bar{n}_y = 0 \tag{21b}$$

$$-\Psi_X\bar{n}_y + \Psi_Y\bar{n}_x = 0 \tag{21c}$$

• *Simply supported edge* (S):

$$W = 0 \tag{22a}$$

$$(\bar{n}_x^2 + v\bar{n}_y^2)\frac{\partial\Psi_x}{\partial X} + (1-v)\bar{n}_x\bar{n}_y\beta\frac{\partial\Psi_x}{\partial Y} + (v\bar{n}_x^2 + \bar{n}_y^2)\beta\frac{\partial\Psi_y}{\partial Y} + (1-v)\bar{n}_x\bar{n}_y\frac{\partial\Psi_y}{\partial X} = 0 \tag{22b}$$

$$-\Psi_{X}\bar{n}_{y}+\Psi_{Y}\bar{n}_{x}=0 \tag{22c}$$

3.3. *Discretization of basic equations and boundary conditions*

We first define the following linear operators which will be required in the discretization of the governing equations, moment and shear resultant equations:

$$\mathscr{R}_1=\frac{\partial^2}{\partial X^2}+\frac{1-\nu}{2}\beta^2\frac{\partial^2}{\partial Y^2}-\xi;\quad \mathscr{R}_2=\frac{\partial^2}{\partial X\partial Y};\quad \mathscr{R}_3=\frac{\partial}{\partial X}; \tag{23a,b,c}$$

$$\mathscr{R}_4=\beta^2\frac{\partial}{\partial Y^2}+\frac{1-\nu}{2}\frac{\partial^2}{\partial X^2}-\xi;\quad \mathscr{R}_5=\frac{\partial}{\partial Y}; \tag{23d,e}$$

$$\mathscr{R}_6=\left(\delta\frac{\partial^2}{\partial X^2}+\gamma\beta\frac{\partial^2}{\partial Y^2}\right); \tag{23f}$$

Using the DC procedures, the normalized governing eqn (14a–c) are discretized as follows:

$$\sum_{j=1}^{n}C_{ij}^{(1)}\Psi_{Xj}+\frac{1+\nu}{2}\beta\sum_{j=1}^{n}C_{ij}^{(2)}\Psi_{Yj}+\xi\delta\sum_{j=1}^{n}C_{ij}^{(3)}W_j=0 \tag{24a}$$

$$\frac{1+\nu}{2}\beta\sum_{j=1}^{n}C_{ij}^{(2)}\Psi_{Xj}+\sum_{j=1}^{n}C_{ij}^{(4)}\Psi_{Yj}+\xi\gamma\sum_{j=1}^{n}C_{ij}^{(5)}W_j=0 \tag{24b}$$

$$\sum_{j=1}^{n}C_{ij}^{(6)}W_j-\sum_{j=1}^{n}C_{ij}^{(3)}\Psi_{Xj}-\beta\sum_{j=1}^{n}C_{ij}^{(5)}\Psi_{Yj}=-Q_d \tag{24c}$$

where $i=1,2,\ldots,n$ and $C_{ij}^{(m)}$ is the cubature weighting coefficients corresponding to the linear operator $\mathscr{R}_m$.

The moment and shear resultant eqns (15–16) are discretized as

$$(\bar{M}_X)_i=-(\sum_{j=1}^{n}C_{ij}^{(3)}\Psi_{Xj}+\nu\beta\sum_{j=1}^{n}C_{ij}^{(5)}\Psi_{Yj}) \tag{25a}$$

$$(\bar{M}_Y)_i=-(\nu\sum_{j=1}^{n}C_{ij}^{(3)}\Psi_{Xj}+\beta\sum_{j=1}^{n}C_{ij}^{(5)}\Psi_{Yj}) \tag{25b}$$

$$(\bar{M}_{XY})_i=-\frac{(1-\nu)}{2}(\beta\sum_{j=1}^{n}C_{ij}^{(5)}\Psi_{Xj}+\sum_{j=1}^{n}C_{ij}^{(3)}\Psi_{Yj}) \tag{25c}$$

$$(\bar{Q}_x)_i=\delta\sum_{j=1}^{n}C_{ij}^{(3)}W_j-\Psi_{Xi} \tag{26a}$$

$$(\bar{Q}_y)_i=\gamma\sum_{j=1}^{n}C_{ij}^{(5)}W_j-\Psi_{Yi} \tag{26b}$$

Let i be the index number of the points on boundary. Using the DC procedures, the normalised boundary conditions for an arbitrary edge (eqns. (21–22)) are discretized as

• *Clamped edge* (C):

$$W_i=0 \tag{27a}$$

$$\Psi_{Xi}\bar{n}_x+\Psi_{Yi}\bar{n}_y=0 \tag{27b}$$

$$-\Psi_{Xi}\bar{n}_y+\Psi_{Yi}\bar{n}_x=0 \tag{27c}$$

• *Simply supported edge* (S):

$$W_i=0 \tag{28a}$$

$$(\bar{n}_x^2+v\bar{n}_y^2)\sum_{j=1}^{n}C_{ij}^{(3)}\Psi_{Xj}+(1-v)\bar{n}_x\bar{n}_y\beta\sum_{j=1}^{n}C_{ij}^{(5)}\Psi_{Xj}$$

$$+(v\bar{n}_x^2+\bar{n}_y^2)\beta\sum_{j=1}^{n}C_{ij}^{(5)}\Psi_{Yj}+(1-v)\bar{n}_x\bar{n}_y\sum_{j=1}^{n}C_{ij}^{(3)}\Psi_{Yj}=0 \tag{28b}$$

$$-\Psi_{Xi}\bar{n}_y+\Psi_{Yi}\bar{n}_x=0 \tag{28c}$$

4. RESULTS AND DISCUSSION

The procedures presented in the preceding sections for the DC method have been applied for solution of several thick plate bending problems. Plates of different shapes such as rectangular plate, triangular plate, trapezoidal plate, skew plate and circular plate subjected to different boundary conditions are selected as the test examples to demonstrate the applicability and accuracy of the method. The results in terms of deflection, bending and twisting moments, and shear forces for homogeneous, isotropic, moderately thick plates with Poisson's ratio $v = 0.3$ are presented. In general, by combining eqn (24) and the boundary conditions given in eqns (27) and (28) results in a $3n$ number of equations with a $3n$ number of unknown coefficients. Thus the values of deflections and rotations can be determined directly by solving this set of algebraic equations. By substituting the computed values of deflections and rotations back to eqns (25) and (26) yields the bending moments $\bar{M}_x$ and $\bar{M}_y$, the twisting moment $\bar{M}_{xy}$ and the shear forces $\bar{Q}_x$ and $\bar{Q}_y$ of the problem.

The numerical results for various example plate problems are tabulated in Tables 1–9 and the comparison of the present results with the exact analytical or numerical values available in the literature, where possible, are made.

4.1. *Rectangular plate*

The mesh pattern employed for rectangular plates is shown in Fig. 1. The numerical results given here include the uniformly loaded rectangular thick plates with CCCC, SSSS and CSCS boundary conditions. The grid points are varying from a range of 25 to 181. The convergence properties of the DC method are studied through the numerical results of each set of the grid points.

Tables 1 and 2 show the deflection, moments, and shear forces at major points of the square plates with different thickness-to-span ratios h/a under the fully clamped and simply supported boundary conditions. The deflections at the plate center for various thickness are compared with those from the exact elasticity solutions by Iyengar *et al.* (1974) and Srinivas *et al.* (1969), the numerical solutions of the higher-order approximate plate theory by Senthilnathan (1989) and the exact solutions of Kirchhoff plate theory by Timoshenko and Woinowsky-Krieger (1959). It is observed that the DC results are in excellent agreement with those from the exact analysis (Iyengar *et al.*, 1974; Srinivas *et al.*, 1969), and more accurate than the numerical values obtained by Senthilnathan (1989) for the case with fully clamped boundary conditions. The discrepancy between the results obtained using 85 grid points and the converged results is within 1%. For the deflections at the central point, 41 grid points provide acceptable results with a maximum discrepancy of 1% for the fully clamped boundary conditions and a maximum discrepancy of 0.16% for the simply supported boundary conditions. For moments at the central point, although a reasonable accurate results can be obtained using 41 grid points for the SSSS boundary conditions, the errors become quite obvious for the CCCC boundary conditions, especially in the case of very small thickness-to-span ratios (e.g. $h/a = 0.01$). Therefore it is concluded here

Table 1. Numerical results and convergence for a square plate with CCCC boundary conditions

h/a	Grid points	$W^{(1)}$ $X=0.5$ $Y=0.5$	$M_x^{(2)}$ $X=0.5$ $Y=0.5$	$M_y^{(2)}$ $X=0.5$ $Y=0.5$	$M_x^{(2)}$ $X=0.0$ $Y=0.5$	$M_y^{(2)}$ $X=0.5$ $Y=0.0$	$Q_x^{(3)}$ $X=0.0$ $Y=0.5$	$Q_y^{(3)}$ $X=0.5$ $Y=0.0$
0.01	25	1.558	3.261	2.550	—	—	—	—
	41	1.279	2.408	2.249	4.444	5.807	0.724	0.182
	61	1.264	2.257	2.265	—	—	—	—
	85	1.269	2.308	2.318	5.136	5.168	0.444	0.432
	113	1.267	2.278	2.271	—	—	—	—
	145	1.268	2.299	2.306	5.135	5.134	0.435	0.434
	181	1.267	2.278	2.246	—	—	—	—
	exact*	1.260	2.30	2.30	5.130	5.130	0.430	0.430
0.05	25	1.521	3.053	2.228	—	—	—	—
	41	1.338	2.383	2.407	4.739	5.515	0.569	0.300
	61	1.318	2.255	2.233	—	—	—	—
	85	1.325	2.314	2.324	5.107	5.135	0.428	0.412
	113	1.326	2.294	2.291	—	—	—	—
	145	1.327	2.300	2.300	5.079	5.080	0.426	0.425
	181	1.327	2.300	2.300	—	—	—	—
	exact†	1.325	—	—	—	—	—	—
	reference‡	1.312	—	—	—	—	—	—
0.10	25	1.604	2.846	2.026	—	—	—	—
	41	1.502	2.373	2.429	4.853	5.219	0.458	0.356
	61	1.494	2.296	2.285	—	—	—	—
	85	1.502	2.320	2.322	4.952	4.954	0.411	0.409
	113	1.504	2.320	2.319	—	—	—	—
	145	1.504	2.320	2.320	4.935	4.936	0.410	0.410
	181	1.505	2.320	2.320	—	—	—	—
	exact†	1.496	—	—	—	—	—	—
	reference‡	1.465	—	—	—	—	—	—
0.20	25	2.170	2.669	1.990	—	—	—	—
	41	2.148	2.353	2.380	4.674	4.788	0.387	0.359
	61	2.170	2.354	2.380	—	—	—	—
	85	2.174	2.358	2.360	4.632	4.629	0.384	0.385
	113	2.168	2.351	2.348	—	—	—	—
	145	2.172	2.357	2.357	4.607	4.603	0.379	0.379
	181	2.172	2.357	2.357	—	—	—	—
	exact†	2.135	—	—	—	—	—	—
	reference‡	2.063	—	—	—	—	—	—

(1) $10^{-3}qa^4/D$; (2) $10^{-2}qa^2$; (3) qa.
* Timoshenko and Woinowsky-Krieger (1959).
† Iyengar *et al.* (1974).
‡ Senthilnathan (1989).

that the recommended smallest grid points for the bending analysis of the plate are 85. Furthermore, it is observed from the comparison studies that a better convergence characteristic of the DC method is achieved for the SSSS boundary conditions than the CCCC boundary conditions.

The results of different grid points for the moderately thick rectangular plate ($h/a = 0.1$) simply supported at $x = 0, a$ and clamped at $y = 0, b$ are presented in Table 3. A comparison of the maximum deflections with those from elasticity solutions (Srinivas *et al.*, 1969) and the numerical solutions of the higher-order approximate plate theory (Senthilnathan, 1989) is carried out. Again, the present results agree well with those from the exact elasticity results with a maximum discrepancy of 1.79%. The results of Senthilnathan (1989), however, have a discrepancy of 4.1%. It should be noted that the error involved here includes not only the numerical error but also the error due to the assumptions made in the plate theories.

Based on the previous convergence studies, the DC method can now be applied to analyze the bending behaviors of thick plates with various kinds of boundary conditions. As an example, we analyze the case of a uniformly loaded square plate with a combination of SCSC boundary conditions here. To obtain accurate results, 145 grid points are used for

Table 2. Numerical results and convergence for a square plate with SSSS boundary condition

h/a	Grid points	$w^{(1)}$ $X=0.5$ $Y=0.5$	$M_x^{(2)}$ $X=0.5$ $Y=0.5$	$M_y^{(2)}$ $X=0.5$ $Y=0.5$	$Q_x^{(3)}$ $X=0.0$ $Y=0.5$	$Q_y^{(3)}$ $X=0.5$ $Y=0.0$
0.01	25	0.4005	5.302	4.605	—	—
	41	0.4060	4.881	4.632	0.537	0.124
	61	0.4065	4.806	4.791	—	—
	85	0.4065	4.784	4.787	0.327	0.348
	113	0.4065	4.791	4.790	—	—
	145	0.4065	4.788	4.789	0.339	0.336
	181	0.4065	4.789	4.789	—	—
	exact*	0.406	4.79	4.79	0.338	0.338
0.05	25	0.4074	5.273	4.599	—	—
	41	0.4119	4.814	4.743	0.419	0.239
	61	0.4117	4.810	4.789	—	—
	85	0.4115	4.786	4.789	0.333	0.343
	113	0.4115	4.786	4.789	—	—
	145	0.4115	4.788	4.789	0.339	0.338
	181	0.4115	4.789	4.789	—	—
	exact†	0.4109	—	—	—	—
	reference‡	0.4114				
0.10	25	0.4262	5.203	4.617	—	—
	41	0.4280	4.792	4.783	0.364	0.294
	61	0.4273	4.795	4.790	—	—
	85	0.4273	4.786	4.789	0.336	0.341
	113	0.4273	4.789	4.789	—	—
	145	0.4273	4.788	4.789	0.333	0.337
	181	0.4273	4.789	4.789	—	—
	exact†	0.4248	—	—	—	—
	reference‡	0.4272	—	—	—	—
0.20	25	0.4918	5.089	4.678	—	
	41	0.4910	4.785	4.793	0.343	0.319
	61	0.4901	4.788	4.787	—	—
	85	0.4904	4.787	4.789	0.338	0.339
	113	0.4906	4.791	4.792	—	—
	145	0.4904	4.789	4.789	0.337	0.337
	181	0.4905	4.789	4.789	—	—
	exact†	0.4861	—	—	—	—
	reference‡	0.4904	—	—	—	—

(1) $10^{-3}qa^4/D$; (2) $10^{-2}qa^2$; (3) qa.
* Timoshenko and Woinowsky-Krieger (1959).
† Srinivas *et al.* (1969).
‡ Senthilnathan (1989).

the following computations. Figures 6–10 show the distributions of deflection w and moment M_x along the center line $Y = 0.5$, twisting moment and shear force along the edge $X = 0.0$ and shear force along the center line $X = 0.5$. The influences of thickness-to-span ratio h/a on the deflection, twisting moment and shear forces along either the edge $X = 0.0$ or the center line are also demonstrated in these figures. The results presented for $h/a = 0.02$ in the figures may be regarded as the ones which are corresponding to the solutions from the Kirchhoff (thin) plate theory.

Figures 6 and 7 illustrate the distributions of the deflection w and the moment M_x along the center line $Y = 0.5$ of the plate. It is clear that a symmetric distribution of w and M_x is expected under a uniform load. As the thickness-to-span ratio h/a increases, both the deflection w and the moment M_x increase. The distributions of the twisting moment M_{xy} and the shear force Q_x along the edge $X = 0.0$ under different loads are presented in Figs 8 and 9. The significant effects of the thickness-to-span ratio h/a on both Q_x and M_{xy} are obvious along the edge near the corner. And in details, with the increase of h/a, the twisting moment M_{xy} increases near the corner but decreases along most part of the edge and when h/a exceeds a certain value, the maximum twisting moment occurs at the corner, whereas the shear force Q_{xy} increases along the whole edge except for the case $h/a = 0.02$ in

Table 3. Numerical results and convergence for a rectangular plate with CSCS boundary conditions ($h/a = 0.1$)

a/b	Grid points	$w^{(1)}$ $X = 0.5$ $Y = 0.5$	$M_x^{(2)}$ $X = 0.5$ $Y = 0.5$	$M_y^{(2)}$ $X = 0.5$ $Y = 0.5$	$M_y^{(2)}$ $X = 0.5$ $Y = 0.0$	$Q_x^{(3)}$ $X = 0.0$ $Y = 0.5$	$Q_x^{(3)}$ $X = 0.5$ $Y = 0.0$
0.5	25	8.902	10.73	4.939	—	—	—
	41	9.003	9.056	5.082	11.75	0.402	0.684
	61	8.791	8.656	4.498	—	—	—
	85	8.859	8.833	4.763	11.52	0.420	0.673
	113	8.859	8.761	4.706	—	—	—
	145	8.857	8.789	4.726	11.42	0.433	0.680
	181	8.852	8.788	4.710	—	—	—
	exact*	8.817	—	—	—	—	—
	reference†	8.876	—	—	—	—	—
1.0	25	2.444	2.105	4.428	—	—	—
	41	2.248	2.702	3.374	6.912	0.176	0.544
	61	2.209	2.540	3.335	—	—	—
	85	2.210	2.590	3.328	6.796	0.252	0.499
	113	2.209	2.579	3.327	—	—	—
	145	2.209	2.580	3.327	6.801	0.248	0.501
	181	2.209	2.579	3.327	—	—	—
	exact*	2.191	—	—	—	—	—
	reference†	2.128	—	—	—	—	—
2.0	25	0.2495	0.3953	1.129	—	—	—
	41	0.2567	0.3961	1.066	2.186	0.157	0.239
	61	0.2562	0.3922	1.067	—	—	—
	85	0.2555	0.3857	1.063	2.102	0.121	0.260
	113	0.2556	0.3833	1.050	—	—	—
	145	0.2555	0.3870	1.064	2.113	0.123	0.258
	181	0.2546	0.3761	1.064	—	—	—
	exact*	0.2510	—	—	—	—	—
	reference†	0.2407	—	—	—	—	—

(1) $10^{-3}qa^4/D$; (2) $10^{-2}qa^2$; (3) qa
* Srinivas *et al.* (1969).
† Senthilnathan (1989).

Table 4. Comparison studies of the present results with the exact solutions (Timoshenko and Woinowsky-Krieger, 1959) for a uniformly loaded simply supported equilateral triangular plate ($h/a = 0.01$ and 166 grid points)

Parameters	Point Locations (X, Y)				
	(0.5, 0.2887)	(0.5, 0.2309)	(0.5, 0.1732)	(0.5, 0.1155)	(0.5, 0.05774)
$w[10^{-2}q_0a^4/(Eh^3)]$	0.6326	0.6063	0.5248	0.3889	0.02078
Exact	0.6319	0.6056	0.5242	0.3887	0.02081
$M_x[10^{-1}q_0a^2]$	0.1805	0.1619	0.1350	0.09930	0.05444
Exact	0.1806	0.1619	0.1350	0.09931	0.05444
$M_y[10^{-1}q_0a^2]$	0.1805	0.1876	0.1770	0.1448	0.08709
Exact	0.1806	0.1876	0.1770	0.1448	0.08711

which the shear force Q_x jumps to a high value. However, the differences among the Q_y distributions along the center line $X = 0.5$ predicted for different h/a are not apparent as shown in Fig. 10.

4.2. *Triangular plate*

The mesh pattern employed for the triangular plates is shown in Fig. 2. First we carried out a comparison study of the present results for the deflections and moments at several locations along $X = 0.5$ with the exact solutions of thin plate theory (Timoshenko and Woinowsky-Krieger, 1959) for a uniformly loaded simply supported equilateral triangular plate ($h/a = 0.01$) in Table 4. The grid points employed here are 166 and the Poisson's ratio used in the calculations is 0.3. An excellent agreement of present results with the exact solutions is observed.

Table 5. Results and convergence for an equilateral triangular plate with different boundary conditions ($\nu = 0.3$)

Boundary conditions	Grid points	$w^{(1)}$ $X = 0.5,\ Y = 0.5$	$M_x^{(2)}$ $X = 0.5,\ Y = 0.5$	$M_y^{(2)}$ $X = 0.5,\ Y = 0.5$
SSS		$h/a = 0.01$		
	109	0.6272	0.1794	0.1797
	136	0.6327	0.1806	0.1805
	166	0.6326	0.1805	0.1805
	199	0.6328	0.1806	0.1805
	exact*	0.6319	0.1806	0.1806
	FEM†	0.6327	0.1801	0.1808
		$h/a = 0.10$		
	109	0.7186	0.1806	0.1806
	136	0.7186	0.1806	0.1806
	166	0.7186	0.1805	0.1806
	199	0.7186	0.1806	0.1806
	FEM†	0.7186	0.1808	0.1808
		$h/a = 0.20$		
	109	0.9788	0.1802	0.1810
	136	0.9783	0.1805	0.1805
	166	0.9786	0.1806	0.1806
	199	0.9800	0.1807	0.1808
	FEM†	0.9786	0.1808	0.1808
CCC		$h/a = 0.10$		
	109	0.2601	0.8720	0.7992
	136	0.2755	0.8415	0.8317
	166	0.2792	0.8410	0.8424
	199	0.2790	0.8403	0.8410
	FEM†	0.2787	0.8432	0.8428
		$h/a = 0.25$		
	109	0.7456	0.8639	0.8704
	136	0.7469	0.8751	0.8751
	166	0.7470	0.8757	0.8753
	199	0.7469	0.8754	0.8750
	FEM†	0.7471	0.8779	0.8775
SCC		$h/a = 0.10$		
	109	0.3658	0.1059	0.0993
	136	0.3627	0.1063	0.0989
	166	0.3625	0.1067	0.0996
	199	0.3624	0.1062	0.0987
	FEM†	0.3624	0.1065	0.0990
		$h/a = 0.25$		
	109	0.8648	0.1052	0.1212
	136	0.8696	0.1060	0.1220
	166	0.8679	0.1057	0.1217
	199	0.8677	0.1057	0.1217
	FEM†	0.8682	0.1060	0.1220

(1) $10^{-2}qa^4/(Eh^3)$; (2) $10^{-1}qa^2$; *Timoshenko and Woinowsky-Krieger (1959); †ANSYS (5.2) software with 2116 grid points.

In Table 5, convergence studies are carried out for deflection w, moments M_x and M_y at the center of the equilateral triangular plate with SSS, CCC and SCC boundary conditions and various thickness-to-span ratios. The grid points used are varying from 109 to 199. The FEM solutions obtained using ANSYS (V.5.2) are also tabulated for the purpose of comparison. The FEM results are obtained with refining the mesh until they are converged. It can be seen that the present results are in good agreement with the FEM solution. It is obvious that different convergence characteristics for different boundary conditions are observed. The SSS plates achieved a better convergence than the CCC and SCC plates with a maximum discrepancy of 0.7%, whereas for the CCC plates with $h/a = 0.10$, the discrepancies between the results obtained using 109 and 199 grid points for the deflection w, moments M_x and M_y at the center of the equilateral triangular plate are 6.77%, 3.7% and 4.8% respectively, but only 1.25% discrepancy in the deflection w, 0.14% discrepancy of the moment M_x and 0.98% discrepancy of the moment M_y are observed when 136 grid points are used. For the CCC plates with $h/a = 0.25$, however, all the discrepancies between the results obtained using 109 and 199 grid points are within 1% except for the moment

Table 6. Numerical results and convergence of central deflections, moments and shear forces of a trapezoidal plate with CCCC boundary condition ($a/b = 1.0$, $c/a = 0.7$)

h/a	Grid points	$w^{(1)}$	$M_x^{(2)}$	$M_y^{(2)}$	$M_{xy}^{(2)}$	$Q_x^{(3)}$	$Q_y^{(3)}$
0.01	25	0.1088	0.2663	0.2510	0.0000	0.0000	6.0560
	41	0.0901	0.2185	0.1636	0.0000	0.0000	2.1300
	61	0.0859	0.2078	0.1652	0.0000	0.0000	0.6526
	85	0.0861	0.2093	0.1634	0.0000	0.0000	0.7282
	113	0.0860	0.2092	0.1633	0.0000	0.0000	0.7660
	145	0.0860	0.2090	0.1634	0.0000	0.0000	0.7758
	FEM*	0.0844	0.2061	0.1650	0.0000	0.0000	0.7701
0.10	25	0.1056	0.2157	0.1709	0.0000	0.0000	0.7043
	41	0.1057	0.2103	0.1687	0.0000	0.0000	0.8302
	61	0.1055	0.2103	0.1678	0.0000	0.0000	0.8079
	85	0.1054	0.2101	0.1678	0.0000	0.0000	0.7979
	113	0.1054	0.2101	0.1678	0.0000	0.0000	0.7940
	145	0.1054	0.2100	0.1678	0.0000	0.0000	0.7923
	FEM*	0.1037	0.2077	0.1685	0.0000	0.0000	0.7903
0.15	25	0.1284	0.2155	0.1697	0.0000	0.0000	0.8606
	41	0.1290	0.2104	0.1720	0.0000	0.0000	0.8510
	61	0.1288	0.2105	0.1714	0.0000	0.0000	0.8193
	85	0.1288	0.2104	0.1714	0.0000	0.0000	0.8163
	113	0.1288	0.2104	0.1714	0.0000	0.0000	0.8110
	145	0.1288	0.2104	0.1714	0.0000	0.0000	0.8115
	FEM*	0.1269	0.2081	0.1720	0.0000	0.0000	0.8102
0.20	25	0.1599	0.2150	0.1707	0.0000	0.0000	0.7452
	41	0.1610	0.2104	0.1753	0.0000	0.0000	0.8718
	61	0.1607	0.2103	0.1750	0.0000	0.0000	0.8277
	85	0.1607	0.2102	0.1750	0.0000	0.0000	0.8279
	113	0.1607	0.2102	0.1750	0.0000	0.0000	0.8370
	145	0.1606	0.2102	0.1750	0.0000	0.0000	0.8367
	FEM*	0.1584	0.2080	0.1754	0.0000	0.0000	0.8349

(1) $10^{-3}qa^4/D$; (2) $10^{-1}qa^2$; (3) $10^{-2}qa$.
* ANSYS (5.2) software with 2626 grid points.

M_x which has 1.3% discrepancy. It can therefore be concluded that for the CCC triangular plate, a better accuracy is obtained when the thickness-to-span ratio increases and for a small thickness-to-span ratio, more grid points are needed in order to obtain the same degree of accuracy.

4.3. *Trapezoidal plate*

The numerical results for the fully clamped trapezoidal plate with $a/b = 1.0$ and $c/a = 0.7$ are given in Table 6. The mesh pattern of the plate is shown in Fig. 3, and the grid points are varying from 25 to 145. The convergence properties and accuracy of the central deflections, bending moments and shear forces for different h/a ratios obtained by the DC method are demonstrated. The converged FEM solutions obtained using ANSYS (V.5.2) software are also presented for the purpose of comparison. A good agreement has been achieved between the present results and the FEM solutions. Similar to the results for the rectangular plate, it is observed that the present results obtained using 85 grid points have attained an acceptable accuracy as compared to those obtained using 145 grid points. It is interesting to note that for all the cases presented here, the convergence properties of the deflection and the moments of the central point are better than that of the shear forces.

4.4. *Skew rhombic plate*

Consider a skew rhombic plate with the length a and the skew angle φ as shown in Fig. 4. A direct comparison study between the present DC results of the deflections, maximum and minimum bending moments at the centroid of the plates with $h/a = 0.01$ and various skew angles and those obtained using other numerical or analytical methods is presented for the fully clamped and simply supported skew plates in Tables 7 and 8 respectively. In both tables, the values used for normalization are taken from the published values of Sengupta (1995), which were obtained using the finite element method based on

Table 7. Convergence studies of a clamped skew rhombic plate ($h/a = 0.01$)

Skew angle (φ)	References	$w_c^{(1)}$	$(M_c)_{max}^{(2)}$	$(M_c)_{min}^{(2)}$
75	61	1.8026	9.1483	8.0733
	85	1.8031	9.1338	8.0953
	113	1.8022	9.1275	8.0951
	145	1.8017	9.1250	8.0930
	Sengupta (1995) (FEM)	1.8114	9.0297	8.0930
	Sengupta (Mindlin Element A)	1.8004	9.1257	8.0855
	Sengupta (Mindlin Element B)	1.7857	8.9492	7.8340
	Butalia *et al.* (1990)	1.7948	9.2207	8.1785
	Kobayashi *et al.* (1995)	1.7966	9.1192	8.0860
60	61	1.2178	7.9454	6.0486
	85	1.2288	7.9298	6.1381
	113	1.2321	7.9231	6.1643
	145	1.2332	7.9201	6.1729
	Sengupta (1995) (FEM)	1.2429	7.8379	6.1199
	Sengupta (Mindlin Element A)	1.2335	7.9161	6.1754
	Sengupta (Mindlin Element B)	1.2275	7.8079	6.0234
	Butalia *et al.* (1990)	1.2281	7.9906	6.2273
	Kobayashi *et al.* (1995)	1.2304	7.9144	6.1760
45	61	0.5773	5.7677	3.6138
	85	0.5932	5.7800	3.7747
	113	0.5991	5.7801	3.8394
	145	0.6018	5.7800	3.8680
	Sengupta (1995) (FEM)	0.6087	5.7178	3.8498
	Sengupta (Mindlin Element A)	0.6051	5.7756	3.9003
	Sengupta (Mindlin Element B)	0.6032	5.7104	3.8030
	Butalia *et al.* (1990)	0.5997	5.8270	3.8933
	Kobayashi *et al.* (1995)	0.6030	5.7768	3.9004
30	61	0.1581	3.1337	1.5142
	85	0.1661	3.1895	1.6488
	113	0.1698	3.2062	1.7208
	145	0.1715	3.2142	1.7208
	Sengupta (1995) (FEM)	0.1746	3.1754	1.7785
	Sengupta (Mindlin Element A)	0.1743	3.2089	1.8205
	Sengupta (Mindlin Element B)	0.1737	3.1722	1.7479
	Butalia *et al.* (1990)	0.1704	3.2603	1.7639
	Kobayashi *et al.* (1995)	0.1732	3.2117	1.8156

(1) $qa^4/(1600D)$; (2) $qa^2/400$.

Mindlin's plate theory. The results in Table 7 show that with the increasing number of grid points from 61 to 145, they converged to the corresponding "accurate" solutions. For all skew angles concerned, the DC results obtained using 145 grid points are in close agreement with those values by Sengupta (1995) and Kobayashi *et al.* (1995). Furthermore, it is observed that with the increasing number of grid points, convergence patterns of the fully clamped moderately thick rhombic plates are monotonous. It is also valid for the results of the simply supported skew plate given in Table 8. However, it is observed that when the skew angle φ is smaller than 45°, the convergence of the present DC results is not quite satisfactory because of the singularity of stresses at the obtuse corners. The results for the plate with $\varphi = 30°$ is in fairly good agreement with those obtained by Butalia *et al.* (1990).

4.5. *Circular plate*

The mesh pattern employed for circular plates with radius a is shown in Fig. 5. Table 9 presents the results and convergence study of the central deflections and bending moments for the simply supported circular plates of various thickness-to-radius ratios, h/a, subjected to a uniformly distributed load. The calculations are carried out over the whole circular domain based on the two dimensional differential equation of the plate. The values of the deflection w and moments M_x and M_y are compared with the solutions obtained by Han and Liew (1997). It is observed that for the plate with thickness-to-radius ratio more than 0.05, 85 grid points are able to provide accurate results, but for the plate with the thickness-to-radius ratio less than 0.05, at least 145 grid points should be employed for the calculations. When the grid points are increased to 145, the exact results are furnished for all

Table 8. Convergence studies of a simply supported skew rhombic plate ($h/a = 0.01$)

Skew angle (φ)	References	$w_c^{(1)}$	$(M_c)_{max}^{(2)}$	$(M_c)_{min}^{(2)}$
75°	61	5.5073	1.8716	1.5967
	85	5.6424	1.8972	1.6371
	113	5.6950	1.9012	1.6608
	145	5.7341	1.9061	1.6741
	Sengupta (1995) (FEM)	5.8172	1.9030	1.6931
	Sengupta (Mindlin Element A)	5.8468	1.9241	1.7097
	Sengupta (Mindlin Element B)	6.0825	1.9650	1.7401
	Butalia *et al.* (1990)	5.8013	1.9207	1.7082
60°	61	3.4138	1.5260	1.1013
	85	3.6755	1.6069	1.1702
	113	3.7791	1.6301	1.2139
	145	3.7591	1.6492	1.2418
	Sengupta (1995) (FEM)	4.1079	1.6909	1.3267
	Sengupta (Mindlin Element A)	4.1123	1.7075	1.3391
	Sengupta (Mindlin Element B)	4.2824	1.7455	1.3670
	Butalia *et al.* (1990)	3.9832	1.6790	1.2980
45°	61	1.5659	1.0720	0.62602
	85	1.7145	1.1429	0.67414
	113	1.7973	1.1776	0.71385
	145	1.8528	1.1988	0.74312
	Sengupta (1995) (FEM)	2.1285	1.2892	0.8787
	Sengupta (Mindlin Element A)	2.1330	1.2995	0.8866
	Sengupta (Mindlin Element B)	2.2028	1.3258	0.9008
	Butalia *et al.* (1990)	1.9125	1.2266	0.7803
30°	61	0.4499	0.5966	0.2677
	85	0.4888	0.6316	0.2882
	113	0.5158	0.6567	0.3066
	145	0.5449	0.6799	0.3321
	Sengupta (Mindlin Element A)	0.6690	0.7734	0.4481
	Sengupta (Mindlin Element B)	0.6841	0.7853	0.4483
	Butalia *et al.* (1990)	0.5194	0.6662	0.3166

(1) $qa^4/(1600D)$; (2) $qa^2/40$.

Table 9. Central deflections and bending moments of a simply supported circular plate

h/a	Grid points	$w^{(1)}$	$M_x^{(2)}$	$M_c^{(2)}$
0.25	85	4.3633	0.20628	0.20628
	145	4.3626	0.20625	0.20625
	181	4.3626	0.20625	0.20625
	Han and Liew (1997)	4.3626	0.20625	0.20625
0.15	85	4.1814	0.20632	0.20632
	145	4.1798	0.20625	0.20625
	181	4.1698	0.20625	0.20625
	Han and Liew (1997)	4.1798	0.20625	0.20625
0.25	85	4.1261	0.20639	0.20639
	145	4.1226	0.20625	0.20625
	181	4.1226	0.20625	0.20625
	Han and Liew (1997)	4.1226	0.20625	0.20625
0.025	85	4.0991	0.20674	0.20666
	145	4.0884	0.20625	0.20625
	181	4.0884	0.20625	0.20625
	Han and Liew (1997)	4.0884	0.20625	0.20625
0.001	145	4.0769	0.20625	0.20625
	181	4.0769	0.20625	0.20625
	Han and Liew (1997)	4.0769	0.20625	0.20625

(1) $qa^4/(64D)$; (2) qa^2.

cases. Furthermore, it is shown that as the value of the thickness-to-radius ratio increases, the deflection at the center of the plate increases whereas the moments M_x and M_y at the center of plate remain unchanged.

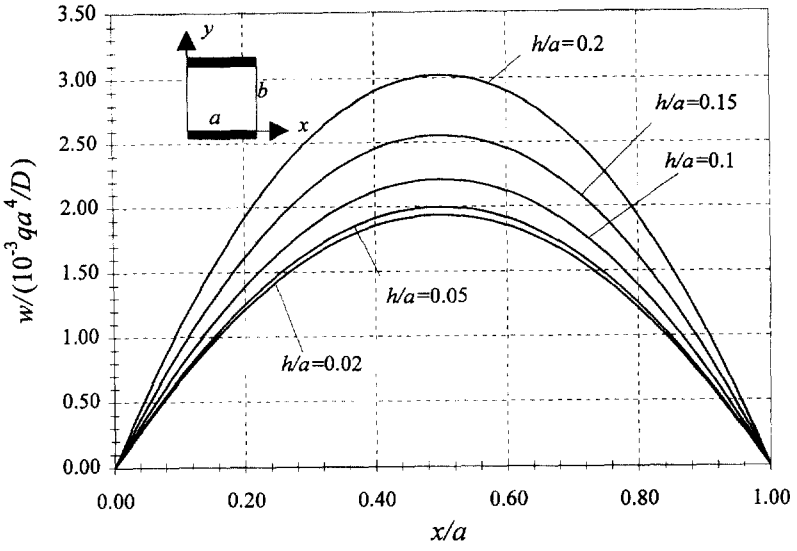

Fig. 6. Variations of w along the centre line $Y = 0.5$ of the uniformly loaded plate ($a/b = 1.0$).

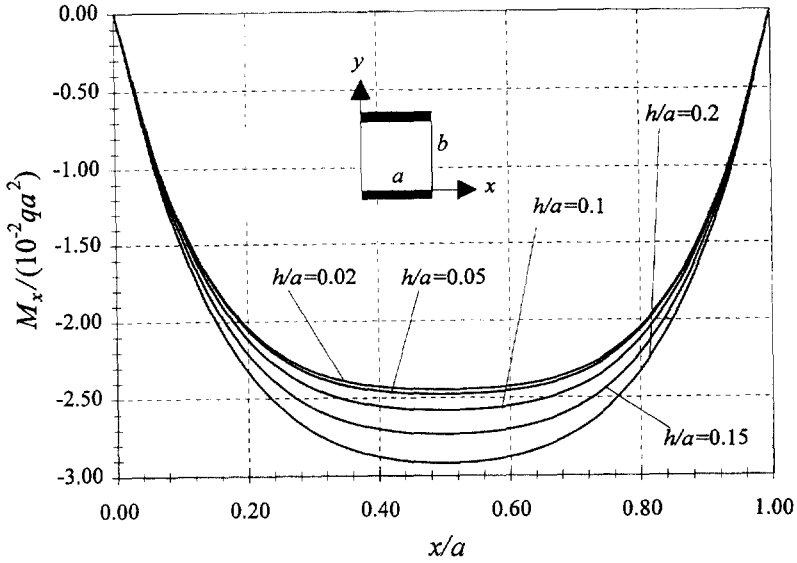

Fig. 7. Variations of M_x along the centre line $Y = 0.5$ of the uniformly loaded plate ($a/b = 1.0$).

5. CONCLUDING REMARKS

In this paper, a first endeavor to exploit the differential cubature method for fundamental solutions of thick plates was presented. Several test examples for different plate shapes have been selected to demonstrate the convergence properties, accuracy and the simplicity in numerical implementation of the DC procedures. The numerical results have been compared with the existing literature. It has been shown that the DC method yields rapid and convergence solutions and these results are in excellent agreement with the exact analytical solutions and other sources of numerical or approximate solutions. Therefore we can conclude that the method can be used as an alternative to the existing numerical methods for the solution of thick plate problem or other similar engineering problems.

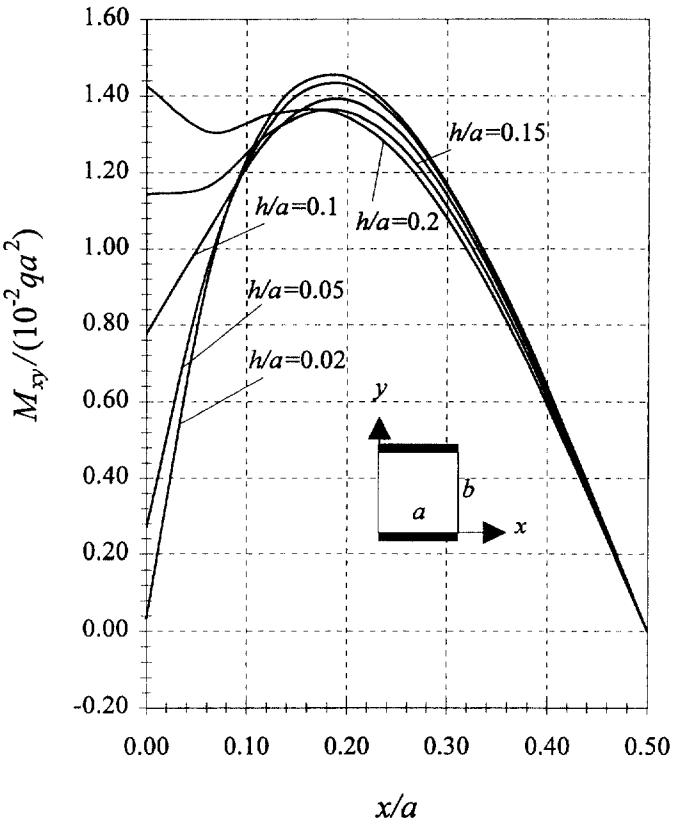

Fig. 8. Variations of M_{xy} along the edge $X = 0.0$ of the uniformly loaded plate ($a/b = 1.0$).

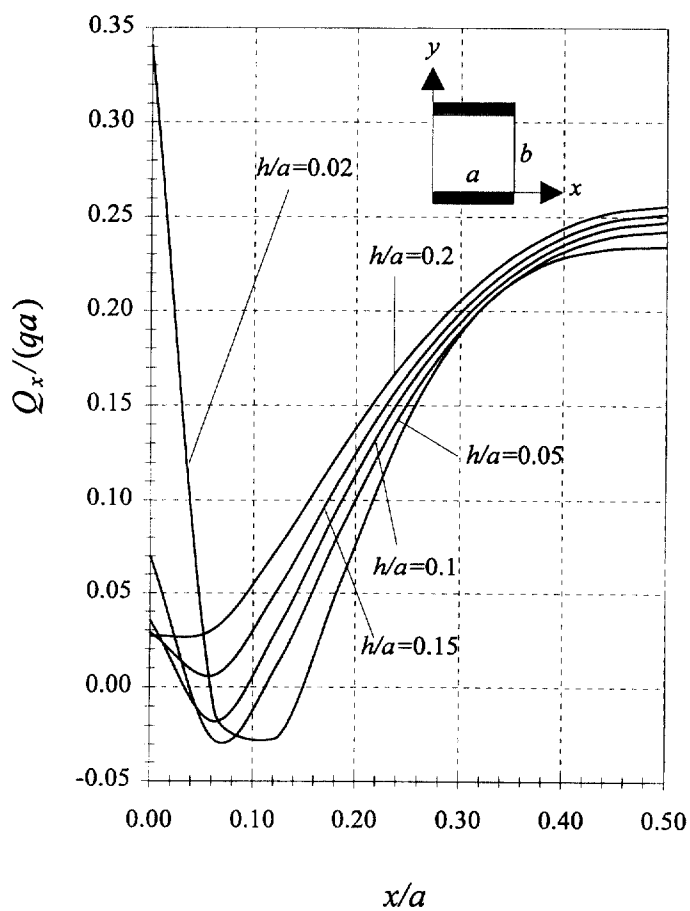

Fig. 9. Variations of Q_x along the edge $X = 0.0$ of the uniformly loaded plate ($a/b = 1.0$).

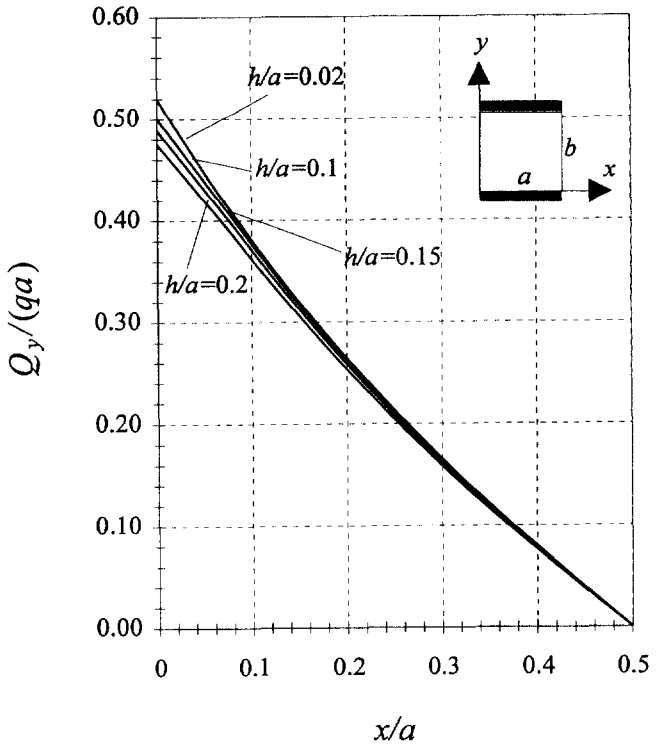

Fig. 10. Variations of Q_y along the centre line $X = 0.5$ of the uniformly loaded plate ($a/b = 1.0$).

REFERENCES

Bellman, R. E. and Casti, J. (1971) Differential quadrature and long-term integration. *Journal of Mathematical Analysis and Applications* **34,** 235–238.

Bellman, R. E. and Casti, J. (1972) Differential quadrature: a technique for the rapid solution of nonlinear partial differential equations. *Journal of Computational Physics* **10,** 40–52.

Bert, C. W., Jang, S. K. and Striz, A. G. (1988) Two new approximate methods for analyzing free vibration of structural components. *AIAA Journal* **26,** 612–618.

Bert, C. W., Jang, S. K. and Striz, A. G. (1989) Nonlinear bending analysis of orthotropic rectangular plates by the method of differential quadrature. *Computational Mechanics* **5,** 217–226.

Butalia, T. S., Kant, T. and Dixit, V.D. (1990) Performance of heteosis element for bending of skew rhombic plates. *Computers and Structures* **34,** 23–49.

Civan, F. and Sliepcevich, C. M. (1984) Differential quadrature for multidimensional problems. *Journal of Mathematical Analysis and Applications* **101,** 423–443.

Civan, F. (1994) Solving multivariable mathematical models by the quadrature and cubature methods. *Numerical Methods for Partial Differential Equations* **10,** 545–567.

Han, J.-B. and Liew, K. M. (1997) An eight-node curvilinear differential quadrature formulation for Reissner/Mindlin plates. *Computer Methods in Applied Mechanics and Engineering* **141,** 265–280.

Iyengar, K. F. S. R., Chadrashekhara, K. and Sebastian, V. K. (1974) On the analysis of thick rectangular plates. *Ing. Arch.* **43,** 317–330.

Kobayashi, H. and Sonoda, K. (1989) Rectangular Mindlin plates on elastic foundations. *International Journal of Mechanical Sciences* **31,** 679–692.

Kobayashi, H., Isshikawa, K. and Tuvey, G. J. (1995) On bending of rhombic plates. *Journal of Structural Engineering*. JSCE **41A,** 41–48.

Liew, K. M., Han, J.-B., Xiao, Z. M. and Du, H. (1996) Differential quadrature method for Mindlin plates on Winkler foundations. *International Journal of Mechanical Sciences* **38,** 405–421.

Liew, K. M. and Han, J.-B. (1997) A four-node differential quadrature method for straight-sided quadrilateral Reissner/Mindlin plates. *Communications in Numerical Methods in Engineering* **13,** 73–81.

Liew, K. M. and Liu, F.-L. (1997) Differential cubature method: a solution technique for Kirchhoff plates of arbitrary shape. *Computer Methods in Applied Mechanics and Engineering* **145,** 1–10.

Mindlin, R. D. (1951) Influence of rotatory inertia and shear in flexural motion of isotropic, elastic plates. Trans. ASME *Journal of Applied Mechanics* **18,** 1031–1036.

Pandya, M. D. and Sherbourne, A. N. (1991) Buckling of anisotropic composite plates under stress gradient. ASCE *Journal of Engineering Mechanics* **117,** 260–275.

Reissner, E. (1945) The effect of transverse shear deformation on the bending of elastic plate. Trans. ASME *Journal of Applied Mechanics* **12,** 69–76.

Sengupta, D. (1995) Performance study of a simple finite element in the analysis of skew rhombic plates. *Computers and Structures* **54,** 1173–1182.

Senthilnathan, N. R. (1989) A simple higher-order shear deformation plate theory. PhD. thesis, The National University of Singapore, Singapore.

Shu, C. and Chew, Y. T. (1994) Application of GDQ scheme to solve incompressible Navier-Stokes Equations in the curvilinear coordinate system. Int. Pacific Air and Space Technology Conf. Proceedings, Singapore, 205–211.

Srinivas, S., Rao, A. K. and Rao, C. V. (1969) Flexure of simply-supported thick homogeneous and laminated rectangular plates. *ZAMM* **49,** 449–458.

Striz, A. G., Chen, W. L. and Bert, C. W. (1994) Static analysis of structures by the quadrature element method (QEM). *International Journal of Solids and Structures* **31,** 2807–2818.

Timoshenko, S. P. and Woinowsky-Krieger, S. (1959) *Theory of Plates and Shells*. McGraw-Hill, New York.